JOURNAL OF SPACECRAFT AND ROCKETS
Vol. 41, No. 3, May–June 2004

Fast Three-Dimensional Modeling of Atomic-Oxygen Undercutting of Protected Polymers

Aaron Snyder* and Bruce A. Banks†
NASA John H. Glenn Research Center at Lewis Field, Cleveland, Ohio 44135

A method is presented to model atomic-oxygen erosion of protected polymers in low Earth orbit. Undercutting of protected polymers by atomic oxygen can occur as a result of the presence of scratch, crack, or pin window defects in the protective coatings. As a means of providing a better understanding of undercutting processes, a fast method of modeling atomic-oxygen undercutting of protected polymers has been developed. Current simulation methods often rely on computationally expensive ray-tracing procedures to track the surface-to-surface movement of individual "atoms." To reduce the burden of time-consuming calculations, the method introduced replaces computationally demanding individual particle simulations by substituting a model that utilizes both a geometric configuration-factor technique, which collectively governs the diffuse transport of atoms between surfaces, and an efficient algorithm, which rapidly computes the cumulative effects stemming from the series of atomic-oxygen collisions at the surfaces of an undercut cavity. This new method facilitates the systematic study of three-dimensional undercutting by allowing rapid simulations to be made over a wide range of erosion parameters.

Nomenclature

A	=	surface area
a, b	=	parameters specifying the dependence of cavity radius upon cavity height
B	=	maximum number of allowed atomic-oxygen bounces in a fluence increment
dA	=	differential area of a surface
E	=	in-space erosion yield for Kapton®
F_{j-i}	=	configuration factor (view factor) from jth area to ith area
F_r	=	fractional reduction in reaction probability per bounce
f^B	=	fraction of atoms reacting after B bounces
f_i^n	=	fraction of atoms reaching ith surface after nth bounce
G	=	volume erosion gain
h	=	cavity height normal to thin-film plane
M	=	number of incremental fluence steps comprising total fluence
N	=	number of surfaces
$\boldsymbol{n}$	=	surface normal
P_r^n	=	probability of erosion reaction for an atom upon nth bounce
P_{rc}	=	probability of atomic-oxygen recombination at coating upon nth bounce
P_{rp}	=	probability of recombination at polymer upon nth bounce
q_i^n	=	probability of atom surviving to reach ith surface after nth bounce
r	=	radius of cavity at a given h
r_1, r_2	=	radius at upper and lower cavity surfaces, respectively
S	=	length of line segment connecting differential areas of two surfaces
V	=	undercut erosion volume
Δ	=	incremental
θ	=	angle between S and surface normal

Subscripts

def	=	defect
i, j	=	surface i or j
k	=	Kapton film
p	=	aggregate of polymer-type surfaces

Superscripts

0	=	initial
$'$	=	value corresponding to incremental fluence
∞	=	asymptotic valued associated with complete thermal accommodation

Received 9 August 2002; revision received 2 June 2003; accepted for publication 8 August 2003.

*Rocket Scientist, Electro-Physics Branch, Power and On-Board Technology Division, 21000 Brookpark Road.

†Chief, Electro-Physics Branch, Power and On-Board Technology Division, 21000 Brookpark Road.

Introduction

UNDERCUTTING of protected polymers by atomic oxygen occurs in low Earth orbit (LEO) because of the presence of scratch, crack, or pin window defects in the protective coatings. Methods to model characteristics of undercutting accurately beneath such defects exist, but because of the extremely complicated nature of the problem fall short of providing a complete representation of the undercutting process. For example, Monte Carlo methods,[1,2] when used in conjunction with ray-tracing procedures, produce remarkably faithful representations, yet are computationally exhaustive for small cell sizes and thus often restricted to two spatial dimensions. A recent method[3] that significantly reduces the computational requirements suffered by ray-tracing codes was used to predict undercutting below pin window defects, and the results were compared against an experimental ground test. This latter method essentially assumes that the cavity walls are uniformly exposed to the atomic-oxygen flux, which limits its applicability to the range of cases where the initial probability of reaction is very low producing an isotropic distribution of atomic oxygen caused by multiple internal scattering. A deficiency for any model is the lack of precise knowledge as to what effective values should apply for atomic-oxygen reaction and recombination rates at polymer and protective coating surfaces. Such lack of knowledge complicates correlation between in-space and ground-based results.

Proper correlation between ground-based systems and flight results are required for meaningful durability studies. A means of establishing such a correlation is the use of computer codes to simulate ground-based and in-space environments. Presently, codes exist that provide such simulations. To advance modeling of three-dimensional undercutting erosion yet minimize computational requirements, a procedure has been developed to provide fast

simulations for a wide variety of conditions. This method shortcuts many computational bottlenecks and avoids lengthy ray-tracing techniques by applying geometric configuration factors to determine the exchange of atoms between cavity surfaces, which in turn are approximated by simple geometric shapes. This method can be used to treat either directed or isotropic arrival of atomic oxygen.

Simple geometries that are easily parameterized were selected. To limit the scope, individual geometries were chosen that exhibit qualities peculiar to directed beam undercutting resulting from a fixed ram direction. Therefore the geometric models used in this paper do not apply to simulation of arbitrary three-dimensional cavities, but are restricted to modeling classes of cavities that exhibit symmetry about an axis or a plane.

The primary goal of this study was to construct a procedure that provides reasonably accurate predictions and serves as a guide for the design of more detailed codes. The central purpose of this paper is to describe the geometric artifices and the physical and computational approaches used here to model undercutting of protected film. Another central purpose is to present a few illustrative examples in order to provide a glimpse of what influence key undercutting parameters have on the rate of undercutting.

Geometric Model

As just mentioned, the code models three-dimensional undercut cavities by using a few prescribed geometries to serve as representative shapes for some of the more simple cavities observed from in-space undercutting below pin window defects. In the model, undercutting occurs directly below a defect present in the upper protective coating of the film. With a double-coated film, a lower protective coating also exists. The protective coating is assumed to be infinitely thin. It is convenient and reasonable to use circular disks to represent the pin window defects. Consistent with this simple defect shape, all model-geometry cavity cross sections in planes parallel to the polymer film are circular. In the present code, four specific geometric classifications exist corresponding to whether the geometric axis is normal or oblique to the surface normal of the film. These four geometries are 1) normal cylinder, 2) normal-truncated cone, 3) oblique cylinder, and 4) oblique-truncated cone. Each of these individual models was chosen to capture a specific set of features characteristic of the posthole-type erosion pattern arising from undercutting caused by directed-beam atomic oxygen. The degree of obliqueness of model 3 or model 4 is determined by the angle that the ram direction deviates from the film's surface-normal direction. The conical geometries allow for modeling of converging and diverging undercut cavities to cover important expected cases encountered in in-space undercutting.

An equation for volume that is valid for the preceding geometric models is given by the following equation:

$$V = (\pi/3)h\left(r_1^2 + r_1 r_2 + r_2^2\right) \tag{1}$$

where r_1 and r_2 are the upper and lower circular disk radii (Fig. 1), which are equal in the case of a cylindrical model. To provide a reasonable characterization, the radial and vertical dimensions of the model cavity must evolve synchronously with cavity volume in a physically realistic manner, for example, the cavity volume must increase monotonically. So as to automate the process and provide a degree of control in specifying model geometries, the radial coordinate is chosen to be a simple function of the cavity height for $h < h_k$, where h_k is the polymer-film thickness. This function is given as follows:

$$r_1 = r_{\text{def}} + ah, \qquad h < h_k \tag{2}$$

For cylindrical geometries the radius is initially equal to the defect radius r_{def} and increases linearly with cavity height for $h < h_k$ depending on the arbitrary scaling parameter a. In the case of conical geometries, an additional parameter b is introduced to relate the radii of the circular disks. Equation (2) is again used to specify r_1, and then r_2 is put in terms of r_1 as given by the following relation:

$$r_2 = r_1 + bh, \qquad h \le h_k \tag{3}$$

As the value of the parameter b is negative, zero, or positive, the conical section is converging, cylindrical, or diverging, respectively. Because the volumes of these models are known functions of the radius and height, the cavity height can be solved in terms of the volume. The protective-coating thickness (typically 0.13 μm) is ignored. In this manner the cavity geometry is specified once the cavity volume is known. The parameters a and b control the cavity aspect ratio and cavity wall slope, respectively. As just mentioned, the degree of variation in the ram direction from normal of the film determines the obliqueness of the model.

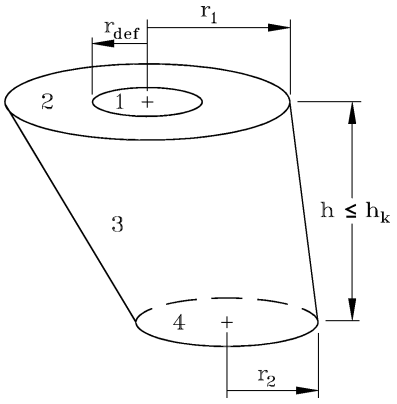

Fig. 1 Typical cavity model geometry for converging, oblique-cone case.

Physical Model

The present model assumes that nonreacting atomic-oxygen atoms reflect off surfaces diffusely, and consequently their movements between surfaces can be treated mathematically like diffuse radiation exchange between surfaces. The fraction of uniform diffuse radiation leaving one surface that reaches another is equivalent to the configuration factor (often referred to as view factor) between two surfaces because it depends solely on the geometric orientation of the surfaces with respect to one another.[4] The geometric dependence of configuration factors can be used to derive algebraic relationships between factors. One pair of configuration factors exists for each pair of finite surfaces. A reciprocity relationship exists for the factors between two finite surfaces. It can be expressed by the following formula:

$$A_i F_{i-j} = A_j F_{j-i} \tag{4}$$

where

$$F_{j-i} = \frac{1}{A_j}\int_{A_i}\int_{A_j} \frac{\cos\theta_i \cos\theta_j}{\pi S^2} dA_j dA_i \tag{5}$$

is the configuration factor from area A_j to area A_i. The angles θ_i and θ_j are the angles between the line segment S, connecting the differential areas dA_i and dA_j, and surface normals $\boldsymbol{n}_i$ and $\boldsymbol{n}_j$, respectively. To complete the general relations among configuration factors needed here, a conservation relation stating that the sum of fractions of emission leaving a surface and arriving at other surfaces of an enclosure (including the emitting surface) must sum to unity is expressed by Eq. (6). With the emitting surface denoted by the subscript index j and the N receiving surfaces of the enclosure identified by the running subscript index i, then the sum of configuration factors can be written compactly as

$$\sum_{i}^{N} F_{j-i} = 1 \tag{6}$$

Given the preceding set of relationships, a complete set of configuration factors can be derived for an enclosed system starting from a relatively small initial subset, which for the geometries used here can be obtained from the existing literature on configuration factors.[4] Next, a detailed description of how to derive additional

configuration factors once a few cataloged factors are available is provided.

An example of the successive steps used to construct a complete set of configuration factors for an enclosure starting from a few known factors is carried out for the case of a truncated cone shown in Fig. 1, which is representative of the simple cavity profiles chosen here for thin film modeling. In this case the cone is converging downward from the defect site. The upper surface of the enclosure is composed of a central disk that represents the defect, and a circular annulus that represents that portion of the upper coating exposed by undercutting. These two areas are denoted as areas 1 and 2, respectively. Connecting the upper and lower planes is the lateral area of the cavity denoted as area 3. The lower disk area is denoted as area 4. For a double-coated film, area 4 represents either a polymer area or a lower protective coating area, depending on whether the cavity has reached the lower coating. Taking into account only those geometric factors between individual elements, there are 16 configuration factors for this case. Suppose F_{4-1} and $F_{4-(1+2)}$ are known or calculated using Eq. (5), where the grouped subscript indices indicate that the corresponding surface is a composite surface. It follows that $F_{4-2} = F_{4-(1+2)} - F_{4-1}$ by the definition of $F_{4-(1+2)}$. In addition, F_{1-1}, F_{2-2}, and F_{4-4} all equal zero by Eq. (5) because they are planar areas with no self-viewing. Analogously, F_{1-2} and F_{2-1} both equal zero. By using reciprocity expressed by Eq. (4), $F_{1-4} = A_4 F_{4-1}/A_1$ and $F_{2-4} = A_4 F_{4-2}/A_2$. By using the conservation equation expressed by Eq. (6), $F_{1-3} = 1 - F_{1-4}$, $F_{2-3} = 1 - F_{2-4}$, and $F_{4-3} = 1 - F_{4-1} - F_{4-2}$. Again using reciprocity, $F_{3-1} = A_1 F_{1-3}/A_3$, $F_{3-2} = A_2 F_{2-3}/A_3$, and $F_{3-4} = A_4 F_{4-3}/A_3$. Finally, by conservation $F_{3-3} = 1 - F_{3-1} - F_{3-2} - F_{3-4}$. Thus, by knowing only a few factors the complete set is found by simple algebra.

Computational Model

The first step in arriving at a computational model is to provide an algorithm to determine the fraction of atoms arriving at a given surface after surviving an arbitrary number of bounces within the enclosure. Let f_i^0 be the fraction of atoms arriving directly through the defect that reaches the ith surface without reflecting off a surface, and let q_i^n be the probability that an atom arriving at the ith surface after n previous cavity bounces will not react, recombine, or exit during the next surface collision, but reflect again. For a polymer surface, $q_i^n = 1 - P_r^n - P_{\text{rp}}$. For a protective-coating surface, where atom loss through efflux is zero, $q_i^n = 1 - P_{\text{rc}}$. The recombination probabilities are held constant throughout a simulation. The fraction of atoms surviving one reflection is $q_i^0 f_i^0$. Thus, by summing over all reflecting surfaces $j = 1, 2$, and $3, \ldots, N$ and employing the configuration factor the fraction of atoms reaching the ith surface after one bounce is given by the following sum:

$$f_i^1 = \sum_j^N F_{j-i} q_j^0 f_j^0 \tag{7}$$

Although the configuration factors must be recalculated as the cavity grows, they are held stationary over a given fluence increment. By telescoping terms from the first bounce, it can be shown that the fraction f_i^n of initial atoms entering the cavity during a given fluence increment that reach the ith surface after n bounces is given by the following summation over the N surfaces:

$$f_i^n = \sum_j^N F_{j-i} q_j^{n-1} f_j^{n-1}, \qquad n = 1, 2, 3, \ldots \tag{8}$$

The fraction of atoms reacting at a polymer surface f_p is found by summing (over the total number of impacts in a fluence increment) the product of the fraction of atoms arriving at the surface times the probability P_r^n of reaction, which in general changes between surface impacts. On average, because of thermal accommodation, kinetic energy is lost following a collision, and this loss is generally reflected in the code by selecting a lower reaction probability for the next impact. The fractional value that the reaction probability per impact is decreased is denoted by F_r. For a large number of bounces, the reaction probability approaches an asymptotic value P_r^∞ consistent with the equilibrium temperature. For convenience, consider the set of all polymer surfaces as being one surface denoted by the subscript p. Then the net fraction of atomic-oxygen atoms reacting at the polymer to cause erosion during a fluence increment consisting of B bounces is given by the following expression:

$$f^B = \sum_{n=1}^{B} P_r^{n-1} \sum_j^N F_{j-p} q_j^{n-1} f_j^{n-1} \tag{9}$$

The total number of atoms reacting during a fluence increment is given by the product of the net fraction of atoms reacting and the total atoms entered, which itself is given by multiplying the incremental atom fluence ΔF by the defect area A_{def}. Continuing in this fashion, the product of the total number of atoms reacting and the erosion yield E (volume/atom) equals the amount of volume erosion ΔV obtained during a fluence increment, which is given by the following:

$$\Delta V = f^B \Delta F A_{\text{def}} E \tag{10}$$

The final undercut volume V is obtained by computing a series of ΔV volumes.

In preparation for discussing results, it is convenient to define the volume erosion gain per incident atom G as the ratio of the volume of undercutting erosion below a defect site to the volume of erosion obtained on the surface of an unprotected "smooth-witness" sample. In terms of simulation parameters, the preceding gain can be determined by dividing the average of the f^B over M fluence increments by the initial reaction probability P_r^0 and is given by

$$G = \frac{\sum f^B}{P_r^0 M} \tag{11}$$

The instantaneous gain G' corresponding to the gain for a single fluence increment is given by

$$G' = f^B \Big/ P_r^0 \tag{12}$$

and provides a normalized erosion rate useful for comparison purposes. When G' equals one, the rate (per atomic oxygen atom) of undercutting erosion equals the rate of erosion of an unprotected smooth sample, that is, the probability of reaction for the average atom is the same. A value of G' greater than one indicates that atoms entering an undercut cavity are more likely, as a result of "geometric trapping," to cause erosion than atoms striking an unprotected surface. Values of G' less than unity can be obtained in the case of well-developed cavities where a sufficient fraction of atoms entering a defect first encounter an exposed lower protective coating and are consequently afforded no "first-strike" chance at producing erosion.

Results and Discussion

Values of the erosion parameters representative of the LEO environment were used in simulations. These nominal values along with other code parameters are listed in Table 1. Any variation from these nominal values is noted in the text as the case occurs. Similar to ground-based experiments, simulated fluence is an effective fluence, equivalent to the atoms per unit area in LEO that would produce the same volume erosion. The in-space erosion yield E for Kapton® representative of LEO is 3×10^{-24} cm^3/atom based on atomic-oxygen energy of 4.5 eV. The fluence value selected is arbitrary but consistent with nominal in-space values incurred over many months of exposure. It is emphasized that the tabulated entry for atomic-oxygen fluence is scaled by polymer-film thickness so that results apply for any film thickness. For example, consider a 0.0025-cm-thickness film, then the incremental normalized fluence, which is listed as 2×10^{22} atoms/cm^2 per cm of film thickness, results in a nonscaled cumulative fluence (composed of 100 fluence increments) of 5×10^{21} atoms/cm^2. The value of the constant a was chosen arbitrarily. The maximum error in the simulated results is approximately $\pm 2\%$ based on step-refinement comparisons.

Table 1 Nominal computational model parameters

Variable	Nominal value
P_r^0	0.11
P_r^∞	0.001
P_{rc}	0.13
P_{rp}	0.24
F_r	0.368
B	500
N_s	100
F	5×10^{21}
E	3×10^{-24}
a	0.0759
b	$\pm r_{\text{def}}/h_k$
r_{def}	$0.1h_k$

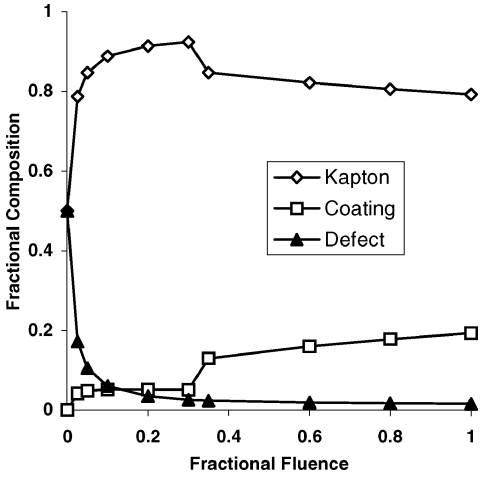

Fig. 2 Variation of cavity surface composition with fluence for normal-cylindrical geometry.

As a cavity evolves, its surface composition affects the rate at which erosion takes place. Obviously, surface composition strongly determines the rate of atomic-oxygen reaction with the polymer, and this reaction rate can be compared to the aggregate loss rate of atomic oxygen by way of recombination and efflux. The degree of influence of cavity composition is constrained by the specified values of the erosion parameters. It is convenient to express the composition of a cavity in terms of the fractional area rather than absolute area. Accordingly, results are presented in Fig. 2 showing the variation of cavity surface composition vs fractional fluence for the normal-cylindrical-geometry model for undercutting below a defect site with $r_{\text{def}} = 0.1h_k$. The shape of each of the curves in this figure is highly representative and typifies, respectively, observed variation in fractional composition with fluence. To clarify the process, stages marked by distinct changes in fractional composition are addressed. At the onset of erosion, the cavity volume is zero, and the exposed area of polymer equals the defect area. Because the defect area is constant, its fractional area initially falls rapidly and then evermore slowly with atomic-oxygen fluence. Meanwhile, the polymer fractional area grows quickly coinciding with a smaller rate of increase in the coating fractional area as a result of erosion peripheral to the defect. Coinciding with the occurrence of the lower base of the cylindrical cavity reaching the bottom surface, the coating fractional area increases rapidly as the lower coating area becomes abruptly exposed, with a corresponding sharp decrease in the polymer fractional area. For larger cavities the coating fractional area monotonically increases at about the rate that the polymer fractional area decreases despite the fact that, with respect to absolute area, both the polymer area and coating area increase with fluence. While the coating area increases as the square of the cavity radius, the polymer area grows only linearly with cavity radius for larger cavity sizes. The cause of the trends seen in Fig. 2 is geometric in nature, whereas the strength of the trends depends on the particular values of the erosion parameters.

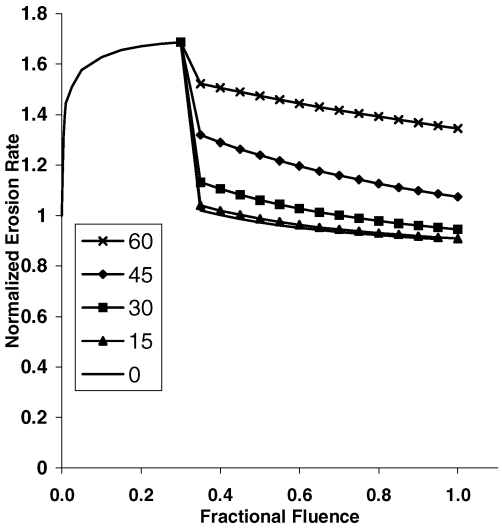

Fig. 3 Dependence of erosion rate upon fluence for various degrees of ram angle.

Knowing the rate of erosion as a function of fluence simplifies establishing cause and effect among various erosion variables. A convenient measure of the rate of cavity erosion is the net reaction probability of an average atomic oxygen atom as supplied by Eq. (9). Another convenient measure is to use G' as given by Eq. (12).

To provide an illustrative example of the type of information achievable by running simulations using this method, results are given (Fig. 3) for the variation of normalized erosion rate G' vs fractional fluence (on a unit area in the plane of the film so that the number of atoms entering a defect is not a function of the ram direction) for various ram angles (degrees from film's normal) for the cylindrical-geometry model for double-coated Kapton, again using nominal parameter values and $r_{\text{def}} = 0.1h_k$. The net reaction probability rises rapidly from its starting value, equal to the initial reaction probability. The reason for this initial increase is that as a cavity enlarges the average atomic-oxygen atom has correspondingly more opportunity to cause erosion as a result of geometric trapping. As a cavity becomes larger, atoms surviving the first impact are less likely to exit the defect upon reflection and likewise for atoms surviving subsequent impacts. As the cavity continues to grow, the tendency of the erosion rate to increase as a result of the trapping effect is increasingly mitigated because of the progressive increase of coating fractional area where no erosion events occur. The sudden dip exhibited in each of the curves presented in Fig. 3, occurring at a fractional fluence equal to approximately 0.3, is caused by the abrupt exposure of the lower coating, as already explained, resulting in a step increase in coating fractional area. This exposure marks the first chance that a fraction of the initial impacts, which in this model are generally more energetic and reactive than subsequent impacts of the atomic oxygen, can occur at a nonpolymer surface. This is why the net reaction probability drops suddenly at this point. The strength of the dip depends strongly on ram angle, with the magnitude decreasing with increasing obliqueness. The reason for this is that a larger ram angle results in a larger distance between the defect site and the exposed area of the lower coating, resulting in a smaller projected solid angle formed by a point at the defect site and the boundary of the exposed lower disk. A smaller solid angle means fewer initial high-energy atoms are lost via recombination by impact with the lower coating, which directly leads to a higher net reaction probability.

To give an example of effects obtained by changing cavity shape, results are given comparing data for the normal-cylinder cavity model with data for the converging and diverging normal-cone cavity models. For the conical geometries, the final wall angle converges or diverges (downward from the defect) by 7.1 deg from axial. A different wall angle would be obtained by choosing a different value for any one of the parameters a, b, or F. For these three geometric models, the variation of normalized erosion rate G' vs fractional fluence is presented in Fig. 4. It is readily seen in Fig. 4 that, whereas

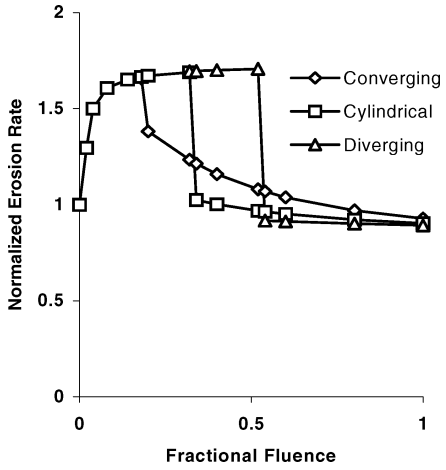

Fig. 4 Dependence of erosion rate upon fluence for converging, cylindrical, and diverging geometries.

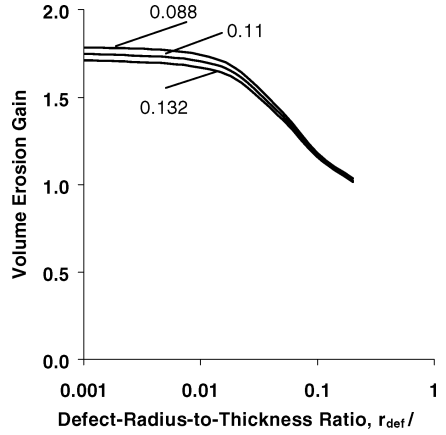

Fig. 5 Dependence of erosion gain upon the defect-radius-to-thickness ratio for various initial reaction probabilities.

each curve is distinguished by the location of a steep dip, the characteristic shape of the curves remains the same for the different geometries. As mentioned earlier, the dip in a curve coincides with the cavity reaching the lower protective coating. The reason that the dip occurs at a lower fluence for a converging cavity is that its volume grows more slowly with cavity height than the other cases, causing it to reach the lower coating first. For the same reason, the cavity of the cylindrical model reaches the lower coating before the cavity of the diverging-cone model.

Two of the most important parameters influencing undercutting erosion are the defect size r_{def} and initial reaction probability P_r^0. To identify any gross effects observed with changes in these two parameters, the variation of final erosion gain G, as a function of the defect-radius-to-thickness ratio r_{def}/h_k, is shown in Fig. 5 for various values of P_r^0 using the normal-cylinder geometry. For these data, r_{def} ranges from $0.2h_k$ to $0.001h_k$. For a given P_r^0, G increases rapidly with decreasing r_{def} until, at a value of r_{def} approximately equal to $0.1h_k$, little increase in G is observed. Gains for the largest defect size $r_{\text{def}} = 0.2h_k$ are close to one, whereas gains for the smallest defect size $r_{\text{def}} = 0.001h_k$ are about 75% greater because of enhanced trapping of the atomic oxygen. It is seen that variations of $\pm 20\%$ from the nominal reaction probability ($P_r^0 = 0.11$) produce respective changes in G of approximately -2.1 and 2.2% for the smallest defects and -0.6 and 1.5% for the largest defects.

As a final example, a comparison of erosion rates is presented for single-coated and double-coated Kapton films. To simulate the effect of having no lower protective coating, the recombination probability is set equal to one at the lower film surface. In Fig. 6 curves of the erosion rate G', as a function of fractional fluence, are shown for single-coated and double-coated Kapton film using the normal-

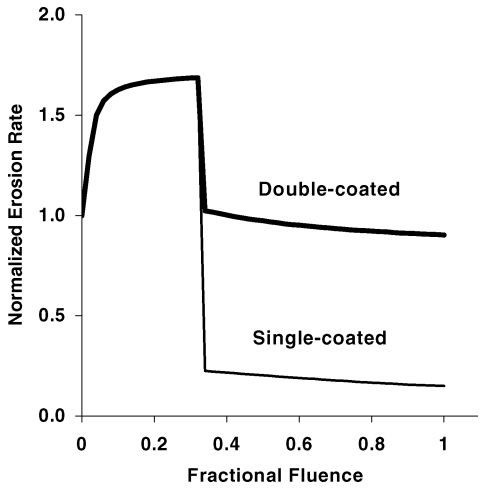

Fig. 6 Variation of erosion rate vs fluence for single-coated and double-coated Kapton.

cylinder model. As expected, the curves are identical until the bottom surface is reached. In the double-coated polymer case, the presence of the lower coating results in additional erosion beyond that obtained in the single-coated case because of reflected atoms.

Conclusions

A new method to simulate three-dimensional undercutting below pin window defects in protected polymer films has been constructed. This method is very fast compared to Monte Carlo methods that employ ray-tracing techniques. To minimize computational requirements, the present method uses a geometric configuration-factor technique to govern the exchange of atoms between surfaces. The model assumes that nonreacting, nonrecombining atoms reflect diffusely off surfaces. The basic equations to derive the configuration factors are given. In addition, the sequence of steps to derive a full set of configuration factors is provided for a representative case. A set of simple geometric shapes are used herein to model undercut cavities. Selection of a particular geometric shape is based on its suitability to faithfully instantiate a set of cavity characteristics. These characteristics include the cavity aspect ratio, cavity obliqueness to the film surface caused by ram angle, and cavity-wall divergence. The equations relating the amount of volume erosion and the rate of volume erosion to the atomic-oxygen fluence are derived. It is demonstrated that by using a suitable set of simple geometries as models simulations are readily obtained spanning a wide range of parameter space. Examples are given that illustrate typical results that can be obtained using the associated computer code. It is the authors' belief that the use of this new technique will enhance the understanding of the undercutting process by allowing quick exploration over a large range of undercutting parameters.

Acknowledgment

The authors thank Edward Sechkar for his contributions to the figures.

References

[1]Banks, B., Stueber, T., Snyder, S., Rutledge, S., and Norris, M., "Atomic Oxygen Erosion Phenomena," American Inst. of Aeronautics Defense and Space Conf., Huntsville, AL, Sept. 1997.

[2]Banks, B., Stueber, T., and Norris, M., "Monte-Carlo Computational Modeling of the Energy Dependence of Atomic Oxygen Undercutting of Protected Polymers," Fourth International Space Conf. ICPMSE-4, Toronto, April 1998.

[3]Snyder, A., and de Groh, K. K., "The Dependence of Atomic Oxygen Undercutting of Protected Polyimide Kapton®H Upon Defect Size," *Proceedings of the 8th ISMSE and 5th ICPMSE*, 2000.

[4]Siegel, R., and Howell, J., *Thermal Radiation Heat Transfer*, 2nd ed., Hemisphere, Washington, DC, 1981, Chap. 7, pp. 187, 188, and Appendix B.

D. Edwards
Associate Editor